



RESEARCH LETTER

10.1002/2014GL061938

Key Points:

- Spectral radiative kernel is developed and validated to get spectral feedback
- Lapse rate and water vapor feedback have different spectral dependence
- Spectral kernel provides new information not available from broadband studies

Supporting Information:

- Readme
- Text S1
- Figure S1
- Figure S2
- Figure S3

Correspondence to:

X. Huang,
xianglei@umich.edu

Citation:

Huang, X., X. Chen, B. J. Soden, and X. Liu (2014), The spectral dimension of longwave feedback in the CMIP3 and CMIP5 experiments, *Geophys. Res. Lett.*, *41*, 7830–7837, doi:10.1002/2014GL061938.

Received 22 SEP 2014

Accepted 6 NOV 2014

Accepted article online 10 NOV 2014

Published online 26 NOV 2014

The spectral dimension of longwave feedback in the CMIP3 and CMIP5 experiments

Xianglei Huang¹, Xiuhong Chen¹, Brian J. Soden², and Xu Liu³

¹Department of Atmospheric, Oceanic, and Space Sciences, University of Michigan, Ann Arbor, Michigan, USA, ²Rosenstiel School for Marine and Atmospheric Science, University of Miami, Miami, Florida, USA, ³NASA Langley Research Center, Hampton, Virginia, USA

Abstract Radiative feedback is normally discussed in terms of the change of broadband flux. Yet it has an intrinsic dimension of spectrum. A set of longwave (LW) spectral radiative kernels (SRKs) is constructed and validated in a similar way as the broadband radiative kernel. The LW broadband feedback derived using this SRK are consistent with those from the broadband radiative kernels. As an application, the SRK is applied to 12 general circulation models (GCMs) from the Coupled Model Intercomparison Project Phase 3 and 12 GCMs from the Coupled Model Intercomparison Project Phase 5 simulations to derive the spectrally resolved Planck, lapse rate, and LW water vapor feedback. The spectral details of the Planck feedback from different GCMs are essentially the same, but the lapse rate and LW water vapor feedback do reveal spectrally dependent difference among GCMs. Spatial distributions of the feedback at different spectral regions are also discussed. The spectral feedback analysis provides us another dimension to understand and evaluate the modeled radiative feedback.

1. Introduction

Radiative feedback is a fundamental concept in the context of climate change, and it is closely related to the climate sensitivity (the global mean surface temperature change in response to a doubling of atmospheric CO₂) [Soden and Held, 2006; Bony et al., 2006; Intergovernmental Panel on Climate Change, 2007, 2013]. Normally, radiative feedback is expressed in Wm⁻²/K, i.e., change of TOA (top of atmosphere) broadband radiative flux due to the response of a particular physical variable to 1 K change of global mean surface temperature. The change of TOA broadband radiative flux is merely the sum of flux changes over all spectral wavelengths. In this regard, the radiative feedback also has a dimension of frequency (or equivalently, wavelength), and we can define the spectral radiative feedback in terms of Wm⁻²/frequency/K. Thus, a series of meaningful questions to ask would be the following: (1) What are the spectral details of each individual feedback such as Planck feedback, lapse rate feedback (denoted as LR for brevity), water vapor (WV) feedback, and cloud feedback? (2) Can such spectral details help us understand and gauge the radiative feedback from different general circulation models (GCMs), especially given the fact that large intermodel spread still exists in their radiative feedback strengths?

To address the aforementioned questions, we develop a spectral radiative kernel (SRK) method to efficiently compute the longwave (LW) spectral feedback. Section 2 describes the construction and validation of the LW SRK. Section 3 describes the spectral details of the Planck, LR, and LW WV feedback of the CMIP3 and CMIP5 (Coupled Model Intercomparison Project Phase 3 and Phase 5) models. The conclusions and further discussions are then summarized in section 4.

2. Spectral Radiative Kernel

2.1. Construction and Benchmark With the Partial Radiative Perturbation Method

The radiative kernel technique has been introduced by Soden and Held [2006], Soden et al. [2008], and Shell et al. [2008] and, since then, has been widely used in the studies of radiative feedback [e.g., Soden and Vecchi, 2011; Sanderson et al., 2010; Dessler, 2010]. This technique employs radiation schemes used in the GCM to compute the TOA broadband flux changes at each grid box in response to a small perturbation to geophysical variables such as temperature or humidity at a given altitude, as well as surface albedo and surface temperature. The perturbation computations are done at high temporal resolutions (e.g., 3-hourly)

and then averaged over a longer time scale (e.g., monthly mean) to form the radiative kernel. Then, in the radiative feedback analysis, the monthly mean kernel is used directly with the monthly mean fields from a GCM simulation to evaluate the radiative feedback strengths. The only exception is the cloud feedback, which has to be obtained indirectly through adjustment methods as detailed in section 5h in *Soden et al.* [2008]. The adjustment methods compute the cloud feedback through adjusting the cloud radiative effect after considering the masking effect of cloud upon the kernels. Further detailed discussion about the broadband kernel techniques can be found in *Soden et al.* [2008], *Shell et al.* [2008], and *Jonko et al.* [2012].

In our study, we follow similar procedures as in *Soden et al.* [2008] to construct the SRK using a spectrally resolved radiative transfer model instead of a particular GCM's broadband radiation scheme. The model is based on *Chen et al.* [2013], which employs PCRTM (principal component-based radiative transfer model) [*Liu et al.*, 2006] as the forward model and takes cloud subgrid variability into account in a similar way as the International Satellite Cloud Climatology Project simulator does [*Klein and Jakob*, 1999]. Unlike traditional channel-based radiative transfer models, which calculate the radiance of each channel separately, the PCRTM calculates the scores (i.e., the coefficients) of precomputed principal components (PCs) in the spectral domain. The PC score contains essential information about the spectral radiances and can be easily calculated by performing radiative transfer calculations at a small number of frequencies. Spectral radiances are then obtained by multiplying the PC scores with prestored PCs. By this approach, the PCRTM achieves both high accuracy and high computational and storage efficiency [*Liu et al.*, 2006; *Chen et al.*, 2013]. The outgoing longwave radiation computed by the forward model agrees with the counterpart directly computed by the Geophysical Fluid Dynamics Laboratory (GFDL) model within 1.8% for all-sky cases and 0.3% for clear-sky cases, as shown in Figure 4 of *Chen et al.* [2013]. Multiple scattering can be included in the PCRTM by incorporating a precomputed look-up table of effective reflectance and transmission of clouds using discrete ordinates radiative transfer model [*Stamnes et al.*, 1988]. Moreover, the PCRTM can simultaneously compute all Jacobians (i.e., the spectral flux changes due to small perturbations of geophysical variables) at the same time when the flux is computed. These features greatly facilitate the construction of SRK.

Soden et al. [2008] suggest that 1 year of simulation is sufficient for computing the kernels. Thus, we use 3-hourly output for the year of 1984 in a 10 year GFDL AM2p12 simulation [*Geophysical Fluid Dynamics Laboratory Global Atmospheric Model Development Team*, 2004] forced by observed sea surface temperature (SST) from 1982 to 1991 (denoted as control run) to construct the longwave SRK at 0.5 cm^{-1} resolution (for better visualization, figures here are all made at 10 cm^{-1} spectral resolution). Since the procedures largely follow *Soden et al.* [2008], the details are put into the supporting information. As an illustration, Figure 1 shows the zonal mean clear-sky and all-sky spectral kernels at four pressure levels (850 hPa, 600 hPa, 300 hPa, and 100 hPa) for both temperature and water vapor. The spectral radiative kernels for the upper tropospheric temperature and humidity are largest in the far-IR band while those for the lower tropospheric temperature and humidity greatest in the window region (where water vapor continuum absorption is important). Comparing the all-sky and clear-sky spectral radiative kernels, the masking effect of clouds is also noticeable, especially for the kernels for the lower tropospheric temperature and humidity.

To validate the SRK, we use the $\pm 2\text{ K}$ SST perturbation simulations [*Cess et al.*, 1990, 1996] by the same GFDL model. Using the PCRTM-based model [*Chen et al.*, 2013], we first apply the PRP (partial radiative perturbation) approach [*Wetherald and Manabe*, 1988] to 3-hourly output to compute the global mean spectral flux differences between $+2\text{ K}$ and -2 K SST perturbation simulations due to the changes of tropospheric temperature, surface temperature, and water vapor, respectively. As in Table 2 of *Soden et al.* [2008], the averages of forward PRP and reverse PRP results are used for the following comparisons. We use the SRK method to compute the same spectral flux changes between the simulations. Figure 2 shows such global mean and annual mean spectral flux differences normalized by the simulated global mean surface temperature difference, for both clear-sky and all-sky spectral kernels. For clear-sky kernel, the broadband flux differences between the SRK and PRP methods are $0.04\text{ Wm}^{-2}\text{ K}^{-1}$ (for temperature changes) and $-0.01\text{ Wm}^{-2}\text{ K}^{-1}$ (for humidity changes). For all-sky kernel, the differences are $0.11\text{ Wm}^{-2}\text{ K}^{-1}$ (for temperature changes) and $-0.01\text{ Wm}^{-2}\text{ K}^{-1}$ (for humidity changes). For all four cases, the fractional differences are smaller than 10%, which is the fractional error of the broadband radiative kernel method with respect to the PRP benchmark

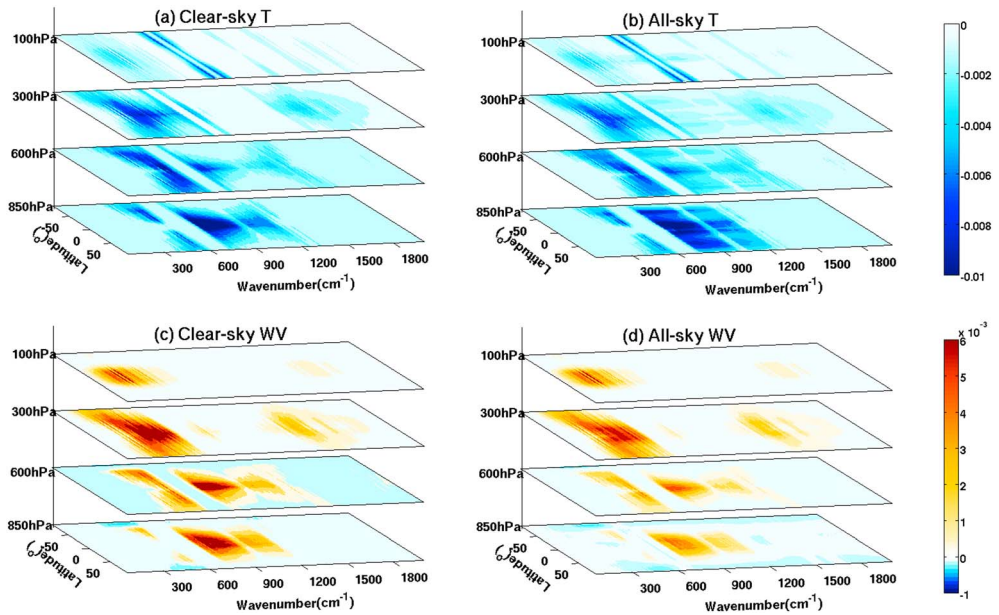


Figure 1. (a) Zonal mean and annual mean clear-sky spectral radiative kernels of temperature at four pressure levels. (b) Same as in Figure 1a except for all-sky kernels. (c and d) Same as in Figures 1a and 1b but for water vapor at the same four pressure levels. All kernels are in the unit of $\text{Wm}^{-2}/10 \text{ cm}^{-1}/\text{K}/100 \text{ hPa}$.

calculated by Soden *et al.* [2008]. For all nonzero flux changes over the 10 cm^{-1} spectral bins from 50 cm^{-1} to 2200 cm^{-1} , the largest fractional difference is $\sim 8\%$, and the averaged fractional difference is only 2.14% for the results shown in Figure 2. Moreover, the differences between the SRK and PRP results have little spectral dependence and are nearly flat around zero for all frequencies (Figures 2e and 2f). These results indicate that for the global mean flux difference, the SRK approach can satisfactorily reproduce the PRP results.

2.2. Nonlinearity of the Spectral Feedback Analysis

The extent to which the radiative kernel technique can be used in the radiative feedback analysis also depends on the linearity of the feedback. To investigate this issue, we use the entire 10 years of output from the same set of $\pm 2 \text{ K}$ SST perturbation simulations described in the previous section. The nonlinearity can be obtained from the residual terms (r_s, r_s^{clr}) of the following two equations for global mean quantities [Zhang *et al.*, 1994],

$$\overline{\Delta R} = \overline{F_{\text{CO}_2}} + (\overline{\Delta R_{T_{\text{air}}}} + \overline{\Delta R_q} + \overline{\Delta R_{T_s}} + \overline{\Delta R_C}) + r_s \tag{1}$$

$$\underbrace{\overline{\Delta R^{\text{clr}}}}_{\text{Total flux change}} = \underbrace{\overline{F_{\text{CO}_2}^{\text{clr}}}}_{\text{CO}_2 \text{ forcing}} + \underbrace{(\overline{\Delta R_{T_{\text{air}}}^{\text{clr}}} + \overline{\Delta R_q^{\text{clr}}} + \overline{\Delta R_{T_s}^{\text{clr}}})}_{\text{feedback}} + \underbrace{r_s^{\text{clr}}}_{\text{residual}} \tag{2}$$

where superscript “clr” denotes clear sky, otherwise all sky. The “total flux change” term on the left-hand side is the TOA incoming longwave flux change directly obtained from the model simulations of $\pm 2 \text{ K}$ SST perturbations. (Following the convention in the feedback analysis, the incoming flux at the TOA is defined as positive flux, and the outgoing flux at the TOA is negative flux.) On the right-hand side, the “ CO_2 forcing” term is zero for the $\pm 2 \text{ k}$ SST perturbation experiment. Among the feedback terms, $\overline{\Delta R_C}$ is the LW cloud radiative feedback computed using the adjustment method as mentioned above, and the rest are all computed using the SRK constructed in section 2.1. Note that the adjustment method in Soden *et al.* [2008] assumes no residual term in the calculation of cloud radiative feedback. Thus, the residual term estimated from equation (1) is affected by the way how cloud radiative feedback is computed. The residual term can then be attributed to the uncertainties in the feedback terms as well as the nonlinearity (because the CO_2 forcing is zero, there is no associated uncertainty). Table 1 summarizes the values of these terms in equations (1) and (2) using all 10 years of $\pm 2 \text{ K}$ SST perturbation runs done by the same GFDL model. For both all-sky and clear-sky cases, the residual term is only $\sim 5\%$ of the feedback term with little year-to-year fluctuation. Thus, we conclude that the

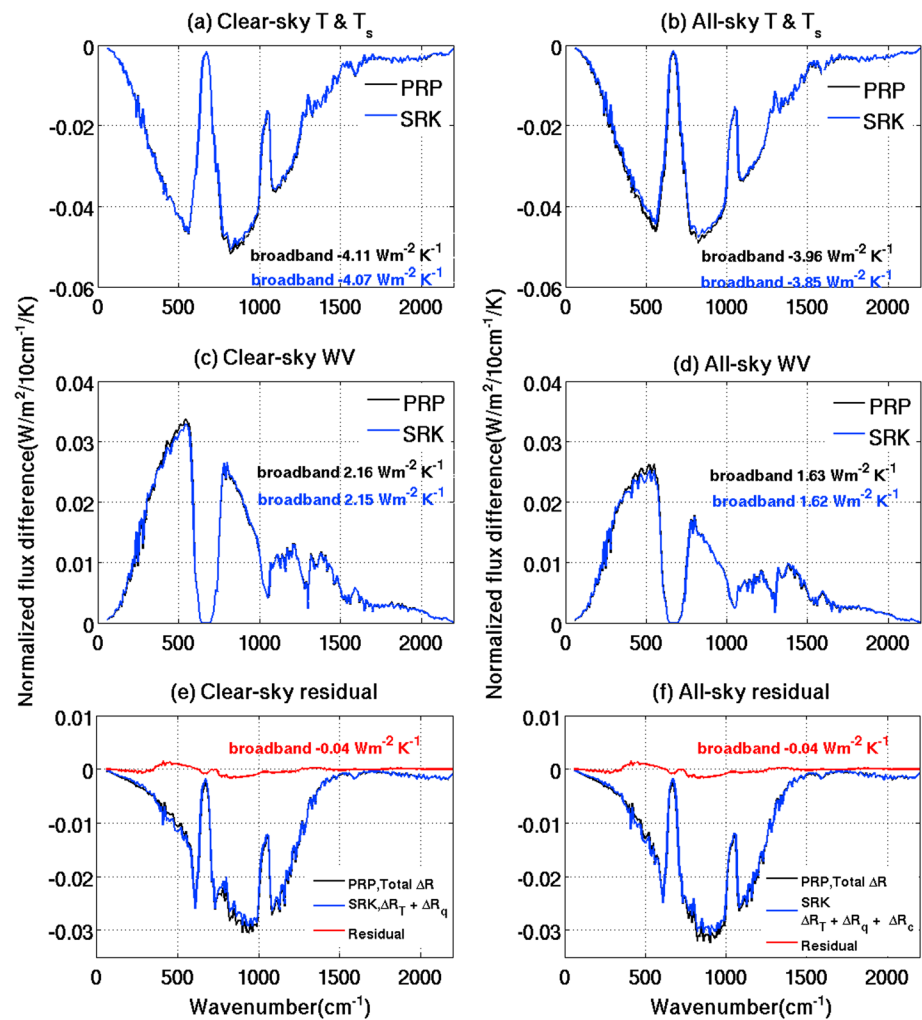


Figure 2. (a) Change of global mean and annual mean clear-sky LW spectral flux due to the temperature differences in response to ± 2 K SST perturbation simulated by the GFDL AM2p12 model. Result from the PRP method is in black line and that from the SRK method in blue line. The spectral flux is plotted for each 10 cm^{-1} interval. (b) Same as in Figure 2a but for the change of all-sky LW spectral flux. (c and d) Same as in Figures 2a and 2b, respectively, but for the change of LW spectral flux due to the water vapor difference. (e) The total spectral flux change computed by the PRP method (black) and by the SRK method (blue). The difference between the two methods is plotted in red. As usual, the change of spectral flux is normalized with respect to the change of global mean surface temperature. The normalized broadband flux change is also given in each panel. Following the convention, the TOA incoming flux is defined as positive. All spectral plots are for 10 cm^{-1} spectral bin from 50 to 2200 cm^{-1} .

nonlinearity contributes only a small fraction (~ 0 – 10%) to the total flux change and the feedback terms derived using the SRK method are useful in the radiative feedback analysis, which is consistent with the conclusions by Soden *et al.* [2008] and Shell *et al.* [2008]. Because the GCM does not calculate spectral flux directly, we cannot use equations (1) and (2) to evaluate the nonlinearity of each spectral channel.

There are two possible sources of nonlinearity: those which result from interactions between different feedback and those which result from the nonlinearity of individual feedback. The SRK method does not account for either nonlinearity, which can therefore be obtained from the residue between the actual TOA flux change computed by the GCM and that estimated by SRK. This is shown in Table 1 to have a value of $-0.09 \text{ Wm}^{-2} \text{ K}^{-1}$. However, the PRP method does take into account the nonlinearity of individual feedback. Using the PRP results from year 1991 (Figure 2 and Table 1), we can estimate that the nonlinearity of individual feedback is $\sim -0.04 \text{ Wm}^{-2} \text{ K}^{-1}$. This then indicates that the nonlinearity due to interactions between feedback is $\sim -0.05 \text{ Wm}^{-2} \text{ K}^{-1}$.

Table 1. Nonlinearity in Longwave (LW) Feedback Process Analysis Based on 10 Year GFDL AM2 Simulations With ± 2 K SST Perturbations as Well as Simulation of Year 1991^a

	Changes of TOA Incoming LW Flux as Computed by the GFDL AM2p12b Model Itself	Changes of TOA Incoming LW Flux as Computed by the PRP Method	CO ₂ Forcing	Feedback	Total Residual Term
Results From All 10 Years					
All sky	-1.94 ± 0.04		0	-1.85 ± 0.04	-0.09 ± 0.01
Clear sky	-2.03 ± 0.03		0	-1.94 ± 0.02	-0.09 ± 0.01
Results From Year 1991 (the Aame Year Used in Figure 2)					
All sky	-1.96	-1.91	0	-1.87	-0.09
Clear sky	-2.02	-1.97	0	-1.93	-0.09

^aThe feedback are obtained using the SRK constructed in section 2. The CO₂ forcing is zero since its concentration is fixed in the simulations. Results from 10 individual years are presented as mean \pm standard deviation. All results are expressed in the units of $\text{Wm}^{-2} \text{K}^{-1}$.

2.3. Comparisons With Feedback Derived From Broadband Radiative Kernel Technique

When the spectral radiative feedback are added together over all LW frequencies, its strength should be consistent with the strength derived using the LW broadband radiative kernel method. This consists of another independent check of the SRK method. We choose 12 GCM outputs from the CMIP3 SRESA1B simulations and apply the SRK as well as two published broadband radiative kernels (*Shell et al.* [2008] referred as the National Center for Atmospheric Research (NCAR) kernel, while *Soden et al.* [2008] referred as the GFDL kernel) to compute the strengths of their LW feedback. For the LW cloud broadband feedback, the adjustment method [*Soden et al.*, 2008] is used to compute the LW cloud broadband feedback once the rest broadband feedback strengths are derived. The results are summarized in Figure S1 and Table S1 in the supporting information. For all GCMs and all four different types of LW feedback (Planck, LR, WV, and cloud), the results from the SRK technique are consistent with the broadband kernel results: the differences between the SRK results and two broadband kernel results are within 10% except a couple of exceptions. Moreover, if we order the GCMs according the magnitudes of their LR (or LW WV or LW cloud) feedback as computed from one method (e.g., the GFDL kernel), such order is largely preserved in results computed using the rest two methods as shown in Figure S1 in the supporting information. This suggests that although the absolute value computed from different kernels might be different, the relative orders of feedback strengths of the 12 GCMs from three different kernel methods (the SRK and two broadband kernels) are highly consistent. This consistency check further corroborates the agreements between our SRK method and the two published broadband kernels. As for the Planck feedback, the orders of feedback strengths from three kernels are not as consistent as those for the rest of the feedback, but the intermodel spread of Planck feedback strength is less than ~5% (compared to ~50% or even bigger spreads in other feedback types).

3. The LW Spectral Feedback of CMIP3 and CMIP5 GCMs

The SRK is then used to compute LW spectral radiative feedback for 12 pairs of GCMs in the CMIP3 and CMIP5 archives that were developed by 12 different climate modeling centers. Relevant details of the GCMs used in this study can be found in the supporting information. For all the CMIP3 and CMIP5 models, simulations of years 1–20 and years 61–80 from the 1%/yr CO₂ increase experiment ([*Taylor et al.*, 2012] known as 1pctto2x run in the CMIP3 and 1pctCO₂ run in the CMIP5, in which all other external forcings except CO₂ are held constant) are used to construct the feedback. Three LW feedback are examined here, all-sky Planck feedback, LR feedback, and WV feedback, and are all computed from surface to the tropopause. For the same reason mentioned in section 2, we do not discuss the LW spectral feedback of clouds because the all-sky spectral flux is not directly available from the GCM; thus, adjustment method cannot be used to obtain the cloud spectral feedback.

Figure 3 displays the aforementioned three types of spectral feedback from the GCMs used in this study. For all three feedback, the spectral component over the center of CO₂ ν_2 band (around 667 cm^{-1}) is zero because this spectral region is only sensitive to the middle stratosphere, and the middle stratosphere is not considered in our feedback analysis. The spectral Planck feedback from all GCMs largely resemble to each

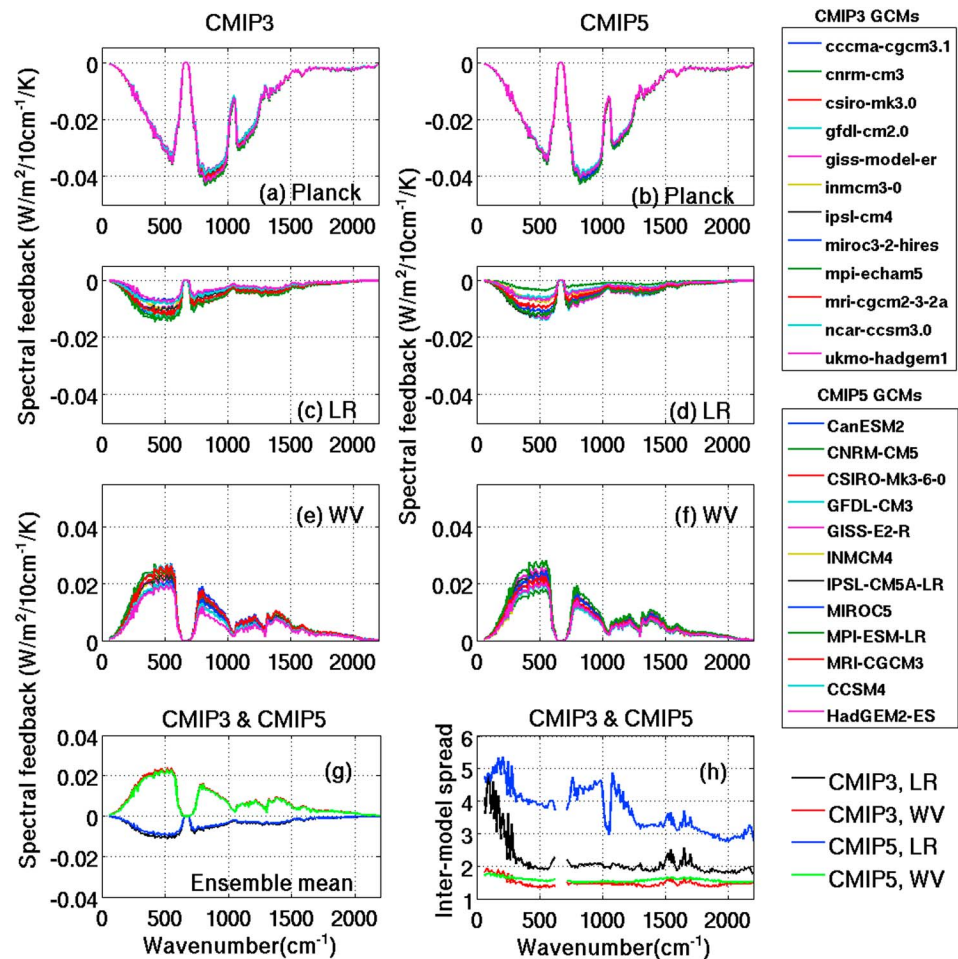


Figure 3. (a) Global mean, all-sky, spectrally resolved Planck feedback based on the 12 CMIP3 GCMs examined in this study. (b) Same as in Figure 3a but based on the 12 CMIP5 GCMs. (c and d) Same as in Figures 3a and 3b but for the lapse rate feedback. (e and f) LW water vapor feedback. (g) The ensemble mean lapse rate feedback of the 12 CMIP3 models (black) and the 12 CMIP5 models (blue) used in this study, as well as the ensemble-mean LW water vapor feedback of the CMIP3 models (red) and the CMIP5 models (green). (h) The intermodel spreads (defined as ratio of maximum to minimum values) of lapse rate feedback among the CMIP3 models and among the CMIP5 models used in this study, as well as the intermodel spreads of LW water vapor feedback. The legends are identical to those in Figure 3g.

other, which should be the case given the definition of the Planck feedback. For both LR and WV feedback, the far IR (0–600 cm⁻¹) contributes to 45–50% of the total broadband feedback strengths, more than any other absorption bands. For the 12 pairs of GCMs examined here, the ensemble mean spectral LR and WV feedback do not change much from the CMIP3 to CMIP5 (Figure 3g). If we use the ratio of maximum to minimum values to represent the intermodel spread, the broadband LR feedback have a spread of 2.07 among the 12 CMIP3 models. For the CMIP5 models, the spread is 3.84. For the LW WV feedback, the spread changes only from 1.37 to 1.56 from the CMIP3 to CMIP5 models examined here. Spectrally, such definition of spread is not applicable to the center of CO₂ band for the reasons mentioned in the beginning of this paragraph. An examination of the spectrally dependent intermodel spread (Figure 3h) reveals that except the spectral region of 0–200 cm⁻¹, the increase of the spread in LR feedback from the CMIP3 to CMIP5 GCMs examined here can be seen in all the rest spectral bands, especially over 200–600 cm⁻¹ in the far IR and 800–980 cm⁻¹ in the window band. In contrast, the intermodel spread of the spectral LW WV feedback has much smaller changes from the CMIP3 to the CMIP5 GCMs examined here. When clear-sky feedback are examined (shown in the supporting information), similar contrasts between LR and LW WV feedback can be seen as well. The anticorrelated strengths between global mean LR and WV feedback are well known

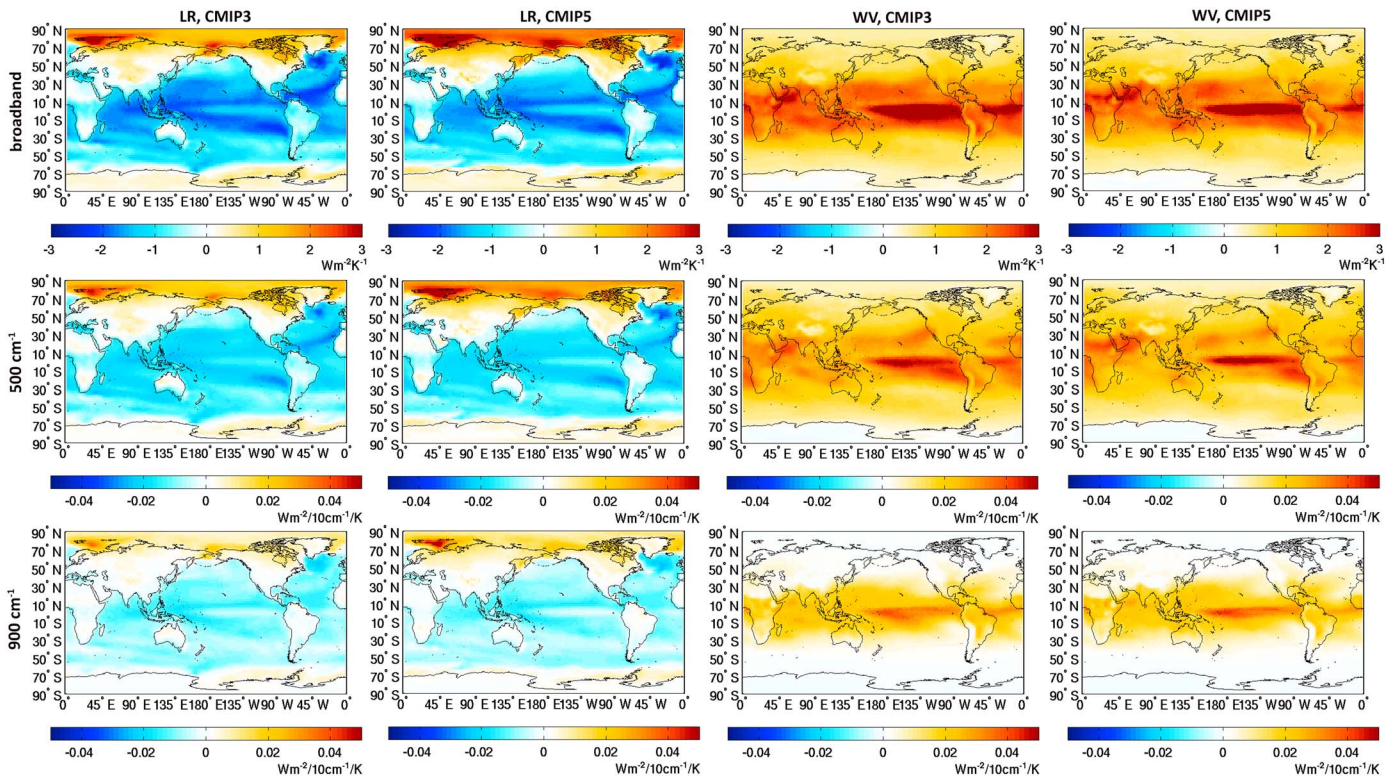


Figure 4. (top row) Ensemble mean spatial patterns of lapse rate and LW water vapor broadband feedback based on the CMIP3 and CMIP5 models used in this study. (middle row) Counterparts over the 500–510 cm^{-1} spectral bin in the far IR. (bottom row) Ensemble mean feedback in 900–910 cm^{-1} spectral bin in the window region. For plots on each row, the color scale is identical.

and have been discussed before [e.g., Cess, 1975; Bony et al., 2006; Soden and Held, 2006]. However, as shown in these figures, the spectral decomposition of the two feedback can reveal more details.

As an illustration of the spatial contrast between the broadband and spectral radiative feedback, the ensemble mean LR and WV feedback maps are shown as Figure 4 for LW broadband and two 10 cm^{-1} spectral bins (one in the far IR and the other in the window band). For the LR feedback in the polar region, the broadband feedback strength dominantly originates from the far-IR region. The LR spectral feedback is positive instead of negative in the polar regions for all LW frequencies. As for LW WV feedback, it is obvious that the window regions contribute much less to the total LW feedback outside the tropics than inside the tropics. This is due to the drier boundary layers in the extratropics than those inside the tropics: the water vapor continuum absorption is most sensitive to the humidity in the boundary layer such that the continuum absorption and emission in the window band are much more important in the tropics than elsewhere. In contrast, the far-IR band is important for the LW WV feedback over the entire globe because it is most sensitive to the humidity in the upper and middle troposphere.

Figure 3 and Figure 4 show that spectral decompositions of the LR and WV feedback can reveal information not directly available from the LW broadband feedback analysis. For example, the all-sky LR feedback for both CanESM2 and INMCM4 models is $-0.55\text{Wm}^{-2}/\text{K}$. But their spectral LR feedback has noticeable difference as shown in Figure 3d and Figure S3 in the supporting information. It is such advantages of spectral feedback that can be further utilized for better understanding difference in the feedback across GCMs.

4. Conclusion and Discussion

Motivated by the success of broadband radiative kernel technique, we develop a set of LW spectral radiative kernel and use it to derive the spectrally resolved LR and LW WV feedback directly from currently available CMIP3 and CMIP5 archives. As discussed by Jonko et al. [2012] regarding the applicability of NCAR kernel for a variety of forcing scenarios, we expect that the SRK constructed here is applicable up to $2 \times \text{CO}_2$ simulations

but not to $4 \times \text{CO}_2$ simulations and beyond. The SRK method is verified against the PRP methods. The broadband feedback computed by the SRK method agree well with the results computed from the published broadband radiative kernels. The spectral decomposition of LW broadband feedback reveals more detail about the feedback of different GCMs. The spatial maps of such spectral feedback demonstrate that in different climate zones, the different spectral regions can contribute differently to the overall LW broadband feedback strengths. These results advocate more analysis of the feedback in the spectral dimension and further exploration how to relate such analysis with the underlying physical processes. The spectral dimension will provide additional and unique insights to the study of radiative feedback, for both longwave and shortwave. Given the global, continuous, and high-quality observations of thermal-IR spectral radiances since 2002 by Atmospheric Infrared Sounder on NASA Aqua, as well as similar observations by Infrared Atmospheric Sounding Interferometer on MetOp and Cross-Scanning Infrared Sounder on Suomi National Polar-Orbiting Partnership, the spectral radiative kernel developed in this study can also be adapted to facilitate the evaluations of GCMs against such satellite observations in the thermal-IR spectral dimension.

Acknowledgments

We wish to thank K. Shell for the thorough and insightful comments, which greatly improved the quality and presentation of our manuscript. We thank the GFDL modeling team for carrying out the Cess ± 2 K SST simulations. We acknowledge the modeling groups, the Program for Climate Model Diagnosis and Intercomparison and the WCRP's Working Group on Coupled Modeling, for their roles in making available the WCRP CMIP3 and CMIP5 multimodel data sets. We are thankful to K. Shell for making her radiative kernels freely available at <http://people.oregonstate.edu/~shellk/kernel.html>. This research is supported by NASA under grants NNX11AE68G and NNX14AF18G awarded to the University of Michigan.

The Editor thanks an anonymous reviewer for assisting in the evaluation of this paper.

References

- Bony, S. R., et al. (2006), How well do we understand and evaluate climate change feedback processes?, *J. Clim.*, *19*, 3445–3482, doi:10.1175/JCLI3819.1.
- Cess, R. D. (1975), Global climate change: An investigation of atmospheric feedback mechanisms, *Tellus*, *27*, 193–198.
- Cess, R. D., et al. (1990), Intercomparison and interpretation of climate feedback processes in 19 atmospheric general circulation models, *J. Geophys. Res.*, *95*, 16,601–16,615, doi:10.1029/JD095iD10p16601.
- Cess, R. D., et al. (1996), Cloud feedback in atmospheric general circulation models: An update, *J. Geophys. Res.*, *101*, 12,791–12,794, doi:10.1029/96JD00822.
- Chen, X. H., X. L. Huang, and X. Liu (2013), Non-negligible effects of cloud vertical overlapping assumptions on longwave spectral fingerprinting studies, *J. Geophys. Res. Atmos.*, *118*, 7309–7320, doi:10.1002/jgrd.50562.
- Dessler, A. E. (2010), A determination of the cloud feedback from climate variations over the past decade, *Science*, *330*, 1523–1527, doi:10.1126/science.1192546.
- Geophysical Fluid Dynamics Laboratory Global Atmospheric Model Development Team (2004), The new GFDL global atmosphere and land model AM2–LM2: Evaluation with prescribed SST simulations, *J. Clim.*, *17*, 4641–4673.
- Intergovernmental Panel on Climate Change (2007), *The Physical Science Basis*, Contribution of Working Group I to the Fourth Assessment Report of the Intergovernmental Panel on Climate Change, edited by S. Solomon et al., 996 pp., Cambridge Univ. Press, Cambridge, U. K., and New York.
- Intergovernmental Panel on Climate Change (2013), *Climate Change 2013: The Physical Science Basis*, Contribution of Working Group I to the Fifth Assessment Report of the Intergovernmental Panel on Climate Change, edited by T. F. Stocker et al., 1535 pp., Cambridge Univ. Press, Cambridge, U. K., and New York.
- Jonko, A., K. Shell, B. Sanderson, and G. Danabasoglu (2012), Climate feedbacks in CCSM3 under changing CO₂ forcing. Part I: adapting the linear radiative kernel technique to feedback calculations for a broad range of forcings, *J. Clim.*, *25*(15), 5260–5272.
- Klein, S. A., and C. Jakob (1999), Validation and sensitivities of frontal clouds simulated by the ECMWF model, *Mon. Weather Rev.*, *127*, 2514–2531.
- Liu, X., W. L. Smith, D. K. Zhou, and A. Larar (2006), Principal component-based radiative transfer model for hyperspectral sensors: Theoretical concept, *Appl. Opt.*, *45*, 201–209.
- Sanderson, B. M., K. M. Shell, and W. Ingram (2010), Climate feedbacks determined using radiative kernels in a multi-thousand member ensemble of AOGCMs, *Clim. Dyn.*, *35*, 1219–1236.
- Shell, K. M., J. T. Kiehl, and C. A. Shields (2008), Using the radiative kernel technique to calculate climate feedbacks in NCAR's Community Atmospheric Model, *J. Clim.*, *21*, 2269–2282.
- Soden, B. J., and I. M. Held (2006), An assessment of climate feedbacks in coupled ocean–atmosphere models, *J. Clim.*, *19*, 3354–3360.
- Soden, B. J., and G. A. Vecchi (2011), The vertical distribution of cloud feedback in coupled ocean–atmosphere models, *Geophys. Res. Lett.*, *38*, L12704, doi:10.1029/2011GL047632.
- Soden, B. J., I. M. Held, R. Colman, K. M. Shell, J. T. Kiehl, and C. A. Shields (2008), Quantifying climate feedbacks using radiative kernels, *J. Clim.*, *21*, 3504–3520.
- Stamnes, K., S. C. Tsay, W. Wiscombe, and K. Jayaweera (1988), A numerically stable algorithm for discrete-ordinate-method radiative transfer in multiple scattering and emitting layered media, *Appl. Opt.*, *27*, 2502–2509.
- Taylor, K. E., R. J. Stouffer, and G. A. Meehl (2012), An overview of CMIP5 and the experiment design, *Bull. Am. Meteorol. Soc.*, *93*, 485–498.
- Wetherald, R., and S. Manabe (1988), Cloud feedback processes in a general circulation model, *J. Atmos. Sci.*, *45*(8), 1397–1416.
- Zhang, M. H., J. J. Hack, J. T. Kiehl, and R. D. Cess (1994), Diagnostic study of climate feedback processes in atmospheric general circulation models, *J. Geophys. Res.*, *99*(D3), 5525–5537, doi:10.1029/93JD03523.